Results

In Fig. 4.5 the ANCORP section and the PRECORP section are shown together with hypocenters of local earthquakes. The sections are displayed according to their relative E-W position in the local migration coordinate system. The *offline stacking* caused apparent vertical discontinuities in the final image, since a lateral amplitude balancing was not applied after stacking. The first 180 km of the ANCORP section shows the following features: Two parallel, clearly distinguishable reflectors are visible at the beginning of the profile. These reflectors, starting at depths of 40 km and 50 km, respectively, are interpreted as the upper and the lower boundary of the oceanic crust. The upper reflector can be traced down to about 80 km depth. This so called Nazca reflector appears very strong over most of its extent, except for small gaps in the area between 20 - 50 km. This is possibly due to the low data quality in this region. At depths greater than 80 km, the reflector image becomes weak and diffuse. It is assumed that this is due to the existence of the strongly reflective Bright Spot visible above between 115 km and 160 km. This so called Quebrada Blanca Bright Spot (QBBS) is located at depths between 15 - 40 km and has a maximum vertical extent of about 15 km. The profile line has a significant N-S component in this region, which enabled an analysis of the cross dip component from N-S oriented sections. The analysis of the 3D volume revealed that the QBBS shows an additional dip component to the north, beside its west dip component observed in the E-W direction (Yoon, 2001). The compilation of the 2D section with local earthquake data shows a good agreement of the hypocenter locations (Gräber and Asch, 1999; Haberland and Rietbrock, 2001) and the position of the Nazca reflector at the beginning of the profile (0 km - 20 km): the hypocenters follow the upper boundary of the oceanic crust. Further to the east of the profile the offset between the hypocenter locations and the Nazca reflector becomes apparently larger ($\geq$ 10 km) with depth. This observation will be discussed in detail later in this chapter.

The 2D depth image of the PRECORP data set shows a short reflector segment at 65 km depth between 50 km and 60 km of the profile (Fig. 4.5). This reflector segment is interpreted as the Nazca reflector. Its appearance outside of the profile line is not surprising considering the dip of the Nazca reflector. Poor data quality weakens the reflections between 60 km and 95 km, but between 95 km and 125 km the Nazca reflector again shows up clearly at depths between 80 - 85 km. Above this reflector - at depths between 15 - 25 km - the so called Calama Bright Spot (CBS) is visible. This bright spot appears with a lateral extension of approximately 15 km and a maximum vertical extension of about 5 - 10 km. It is not clear whether the lateral extension of the bright spot is real or

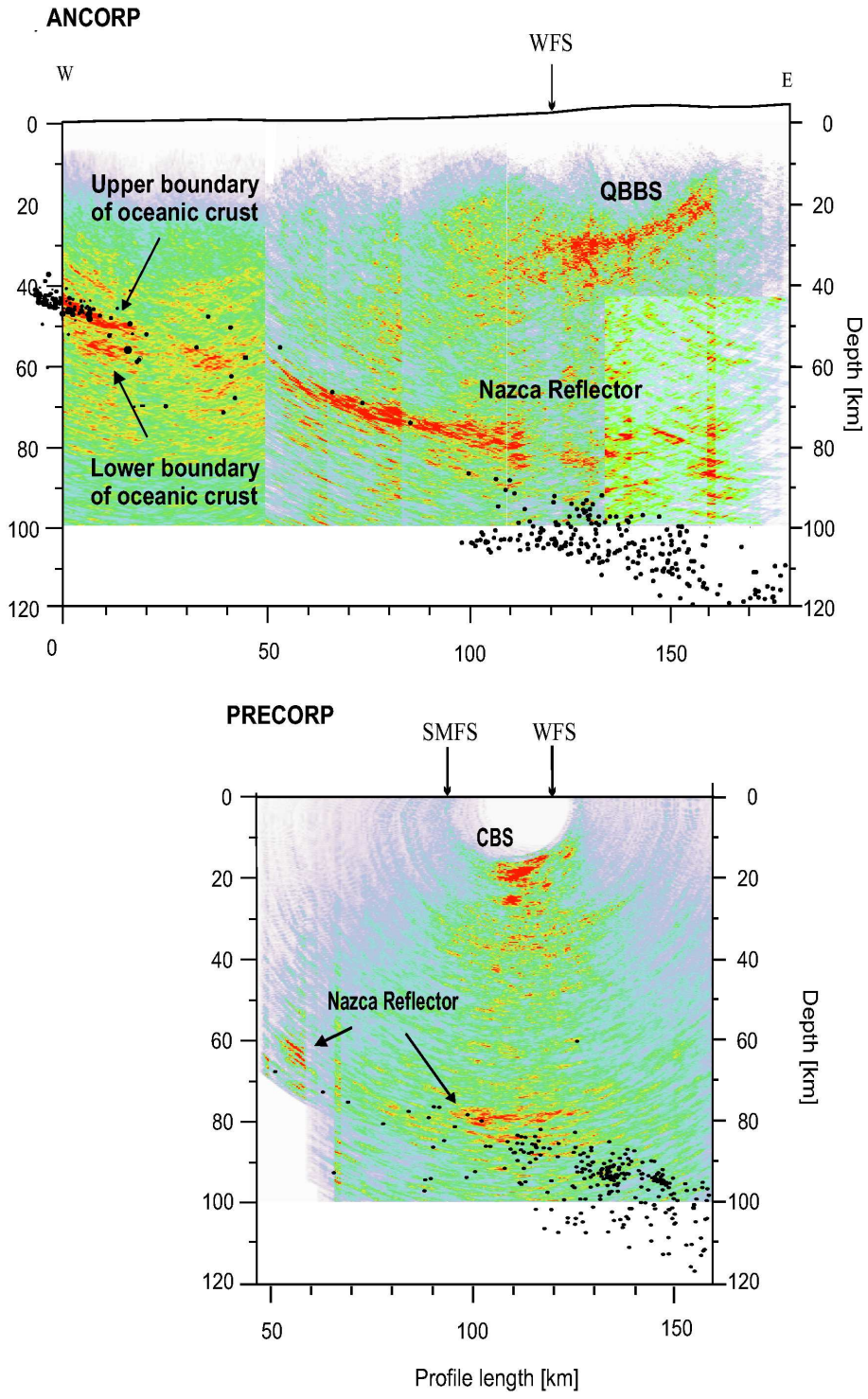

Figure 4.5: 2D ANCORP and PRECORP depth sections. The hypocenter locations are indicated by black dots (Gräber and Asch (1999)).

appears limited due to the recording geometry. An offset between the hypocenter locations and the Nazca reflector is visible, but the amount is less compared to the offset observed in the ANCORP image.

A compilation of the ANCORP and the PRECORP sections shows that the positions of the Nazca reflectors of both sections fit spatially well (Fig. 4.6). This section was obtained by pasting two segments of the PRECORP image into the ANCORP section at their corresponding E-W positions. The two parts show a dipping Nazca reflector segment at the beginning and the CBS as well as the deep Nazca reflector in the middle of the PRECORP section. The dip of the Nazca reflector in the PRECORP image at 50 km is slightly steeper, which might be due to low data coverage in this part. However, from this image it can be assumed that the subduction angle and the depth of the oceanic plate do not significantly change over that distance of about 160 km in N-S direction. The composition clearly shows the relative locations of the QBBS and the CBS in depth and in E-W direction. The CBS is located about 10 - 15 km closer to the surface and is located nearly 15 km further to the west regarding the QBBS. The results will be discussed in details in the following.

Discussion

The application of Kirchhoff prestack depth migration to the ANCORP'96 data set provided images of the subduction zone over a large depth range with interesting details. First, the 2D section shows the oceanic crust with thickness of about 7 km. This corresponds to the thickness of oceanic crust derived from wide-angle refraction measurements in this region (Patzwahl et al., 1999). Second, the reflections from the Nazca reflector do not break down completely at a depth of 80 km - as seen in previous poststack images (ANCORP Working Group, 2003), but continue down to greater depths. Furthermore, the ANCORP section seems to impose that the nature of reflectivity of the Nazca reflector changes with depth, as the reflections appear very sharp at depths between 40 km and 60 km, but become disrupted and blurred at depths greater than 70 km. However, it is assumed that this phenomenon is probably due to the influence of the heterogeneous overburden on the seismic signal, but in principle can also be due to the complexity of the reflector at greater depths itself. The compilation with local earthquake data shows a good spatial agreement between the hypocenters and the upper boundary of the oceanic crust at the beginning of the profile. At greater depths the hypocenter locations and the Nazca reflector show an increased offset. A slightly smaller offset is observed in the PRECORP image. Both depth sections exhibit a bright spot in the fore-arc: the Quebrada

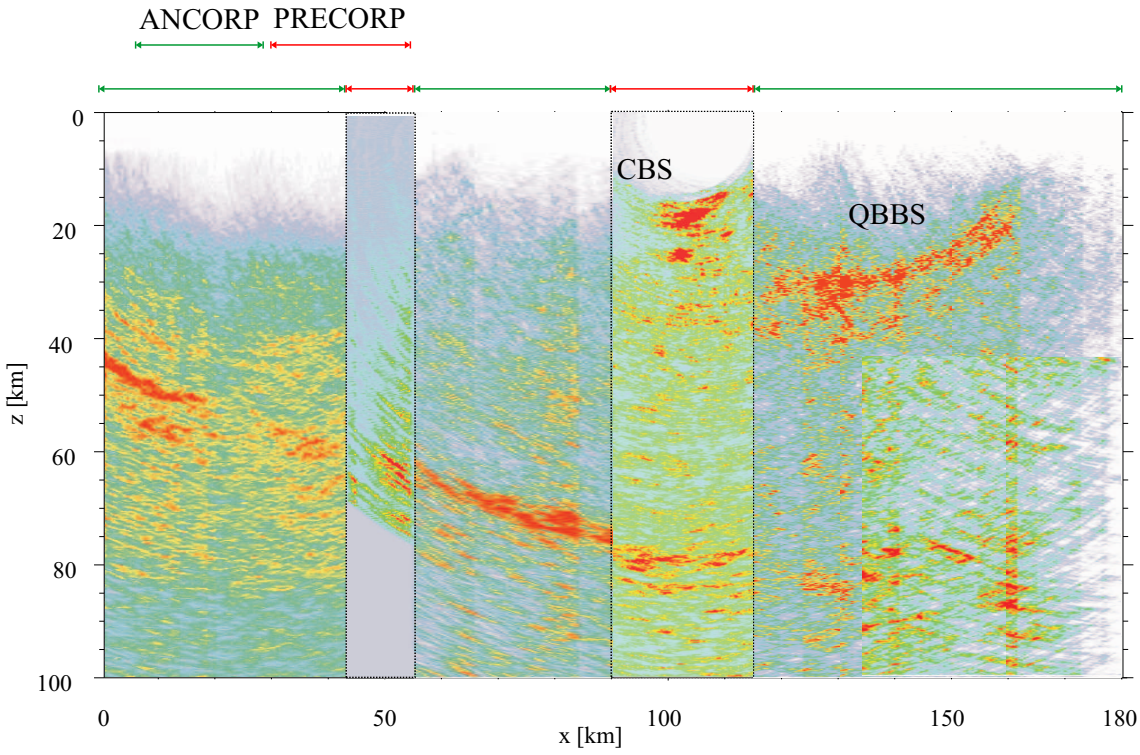

Figure 4.6: Composition of the ANCORP and the PRECORP section. Two parts of the PRECORP image are pasted into the ANCORP image according to their local coordinates. The green and red horizontal arrows on top indicate the origin of the data, representing ANCORP and PRECORP, respectively. The position of the PRECORP-Nazca reflector at 50 km fits spatially well with the Nazca reflector image of the ANCORP data. The deep Nazca reflector in the PRECORP section is located less than a few kilometers deeper than the reflector in the ANCORP section. The QBBS (ANCORP) is located east of the CBS (PRECORP) and is imaged about 10 to 15 km deeper. The latter observation agrees with the hypothesis that the QBBS, which shows a north dipping component, and the CBS are related to the same structure.

Blanca Bright Spot (QBBS) in the ANCORP section and the Calama Bright Spot (CBS) in the PRECORP section. The QBBS, located at depths between 15 - 40 km and dips to the west as well as to the north. Interestingly, the western edge of the QBBS correlates almost with the north-south striking Precordilleran Fault System (PFS), which locally splits up into the Sierra-de-Moreno Fault System (SMFS, Fig. 4.3) and the West Fissure system (WFS) further to the south (Scheuber and Reutter, 1992; Günther et al., 1997). The CBS, located nearly 160 km further to the south, is located about 10 - 15 km closer to the surface and shows a west dipping component. It is located nearly 15 km further to the west regarding the QBBS (Fig. 4.5), east of the SMFS, but west of the WFS. Thus, both bright spots appear delimited by the Precordilleran Fault System, but with changes in spatial relationship. The north dipping component of the QBBS and the upward shift of the CBS indicate that both bright spots are somehow connected, or at least are caused by the same geological structure or processes. Nevertheless, the origin and the geological nature of these bright spots are not fully explained yet.

The offset between the Nazca reflector and the hypocenters at depths greater than 80 km is interpreted in the following way (ANCORP Working Group, 2003): At these depths the Nazca reflector does not represent the top of the oceanic crust, but the reflections are caused by trapped fluids and sheared zones at the serpentinisation front in the mantle wedge above. The observed seismicity is attributed to dehydration embrittlement in the oceanic crust. Assuming that the observed offset is real, this explanation is reasonable and sufficient. However, it seems also possible that the observed offset is an apparent feature that results from the compilation of two data sets that were processed using different velocity models: The reflection data were migrated using the velocity model from refraction data analysis (Lüth, 2000), the hypocenters were localised using a tomography model. In order to investigate this possibility, the ANCORP data were migrated using two velocity models obtained from tomographic inversion. These results and the application of the RIS method to the ANCORP data set will be presented in the following sections. The latter will enable an alternative interpretation with regard to the mentioned offset, as well as to the structures of the mantle wedge above the oceanic crust.

4.2.3 Migration of the ANCORP data with different velocity models

The depth images presented in the last section revealed an offset between the Nazca reflector and the local hypocenters. A structural and petrophysical interpretation of the phenomenon was presented by ANCORP Working Group (2003). The image of the ANCORP reflection data was obtained from migration using the velocity model derived from

refraction data analysis (ANCORP Working Group, 1999; Yoon et al., 2003). However, the hypocenter locations were obtained using a velocity model derived from local earthquake tomography. The question remains whether this offset is due to the differences of the used velocity models. To investigate the latter the ANCORP depth images were recalculated using two tomography velocity models.

The velocity models

In the following the velocity model from refraction data analysis (Lüth, 2000) will be referred to as model 1. The recalculation of the migrated sections was performed using two velocity models that were derived independently from different tomographic inversion schemes, but using the same data set. Technical details on the inversion methods will not be discussed here. One tomography model, which will be referred as model 2 in the following, was provided by Rietbrock and Haberland (2001), the second one (model 3) was provided by Koulakov (pers. comm., 2004). All models are shown in Fig. 4.7.

Travel times from a hypocenter at a depth of 90 km in the central part of the model ($x = 150$ km) to the surface ($z = 0$ km) were calculated to compare the average velocities in the models (Fig. 4.8). The comparison shows that the largest travel times are obtained for model 3 and the shortest travel times for model 2. The travel times for model 1 are almost everywhere located between the travel times of model 2 and model 3. The maximum travel time differences for model 3, model 2 are about 1.5 s ($x = 190$ km), and 1 s for model 1 and model 3 ($x = 120$ km). However, the travel time differences for model 1 and model 2 are small between $x = 100$ - 150 km. From this result it can be concluded that the average velocities are highest in model 2 and lowest in model 3, respectively. Strikingly, both tomography models deviate from model 1 in different direction. This is surprising as both models are based on the same data.

Results and discussion

The migration and stacking procedure during the recalculation of the images followed exactly the same processing scheme as described in section 4.2.2. The top section in Fig. 4.9 shows the ANCORP section calculated using model 1 for comparison (Yoon et al., 2003). A description of this depth section was given in section 4.2.2. The recalculated sections are displayed in the middle and in the bottom of Fig. 4.9. All sections are displayed using the same amplitude scaling. The descriptions of the recalculated images will mainly focus on the appearance of the Nazca reflector.

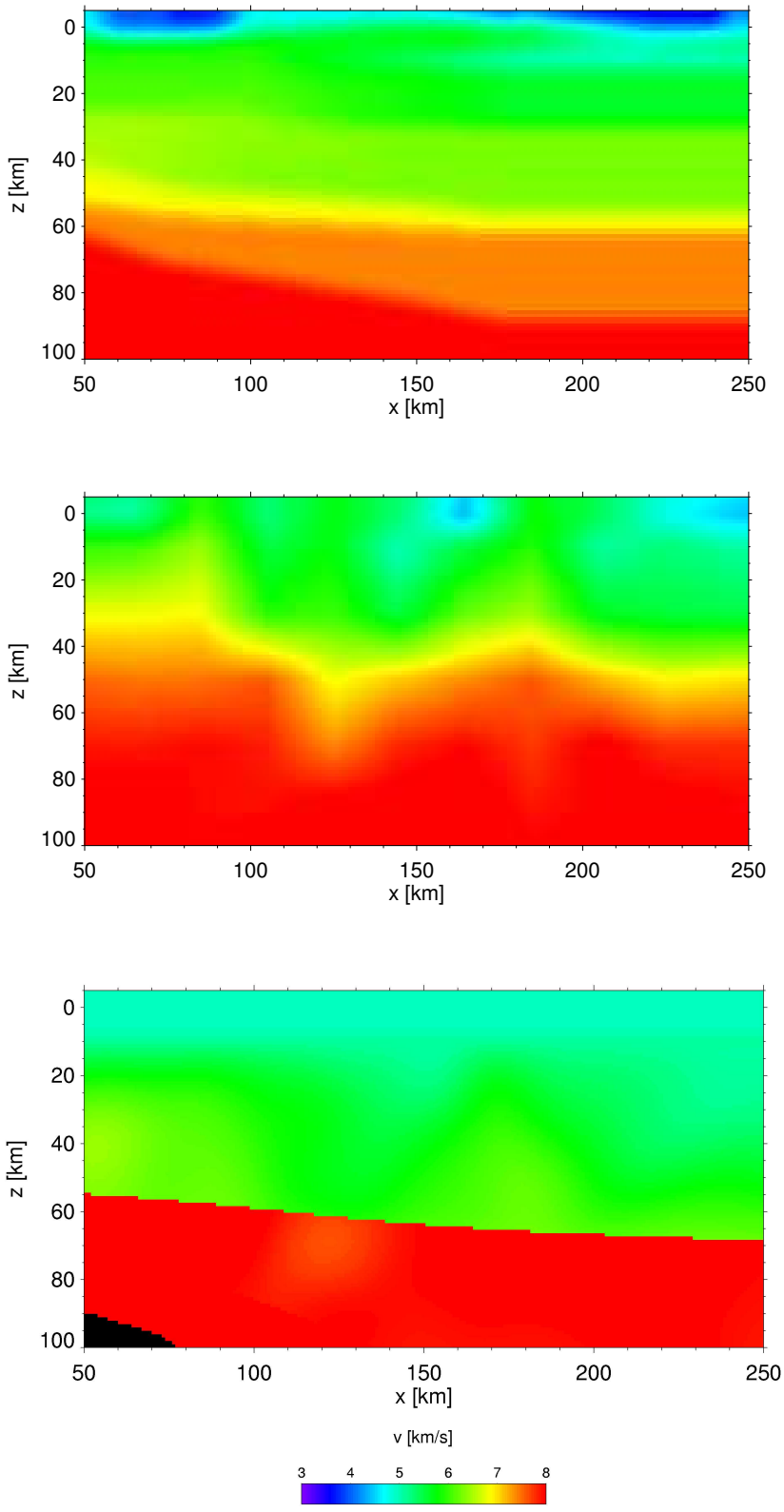

Figure 4.7: Velocity models used for migration of the ANCORP data set. **Top:** Model 1 from refraction data analysis (Lüth, 2000). **Middle:** Model 2 from local earthquake tomography (Rietbrock and Haberland, 2001). **Bottom:** Model 3 from local earthquake tomography (Koulakov, pers. comm. 2004).

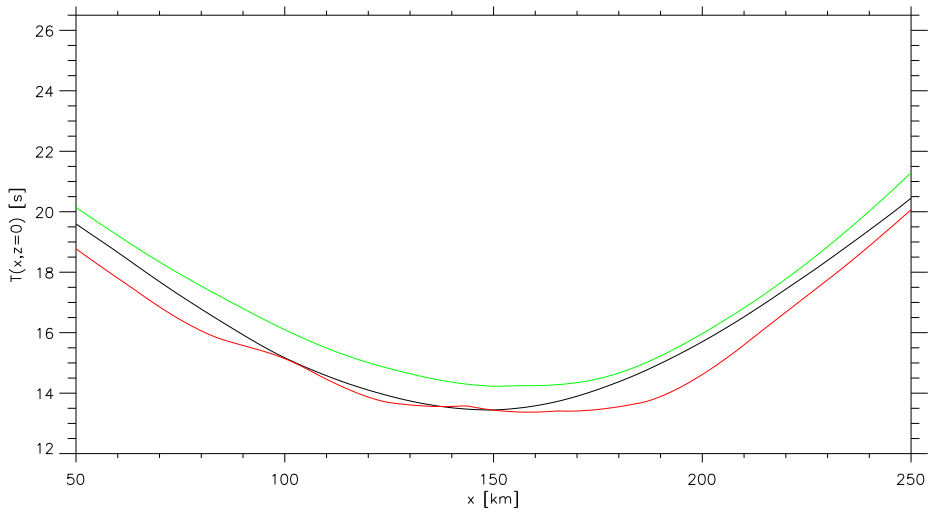

Figure 4.8: Travel time curves calculated for a hypocenter located at a depth of 90 km in the middle of the profile. Black - Model 1; Red - Model 2; Green - Model 3.

The middle section in Fig. 4.9 shows the image calculated for model 2. At the beginning of the section the reflections from the top and the bottom of the oceanic crust are visible at depths of 44 km and 52 km, respectively. The continental Moho is weakly visible as a thin bended reflector at depths between 35 - 40 km. Between $x = 20$ - 50 km the depth section hardly reveals any pronounced coherent reflections and appears dominated by migration noise. Between $x = 50$ - 75 km two relatively thin parallel reflectors are clearly visible at depths between 70 - 80 km (Nazca reflector). They show approximately the same dip as the reflections from the oceanic crust at the beginning of the profile. Between $x = 75$ - 110 km the Nazca reflector appears strong and almost horizontal. Its thickness varies between 7 - 12 km. The upper and the lower boundary are located at depths of 70 km and 82 km, respectively. At $x = 100$ km the Nazca reflector becomes disrupted and finally disappears at ca. $x = 113$ km.

The depth section calculated for model 3 is shown in the bottom of Fig. 4.9. The reflections from the oceanic crust at the beginning of the profile are located at depths of 35 km and 45 km. These reflections are less pronounced and less coherent than in the other two images. The region between $x = 20$ - 50 km indicates weak reflections, which appear similar to those in the top section of Fig. 4.9. At $x = 55$ km two thin parallel reflectors are visible at 62 km and 68 km depth. These reflectors merge with the stronger and thick reflector at $x = 70$ km. Between $x = 70$ - 100 km the reflector appears strong with a slightly east dipping component. Its thickness is about 10 km, its upper and lower

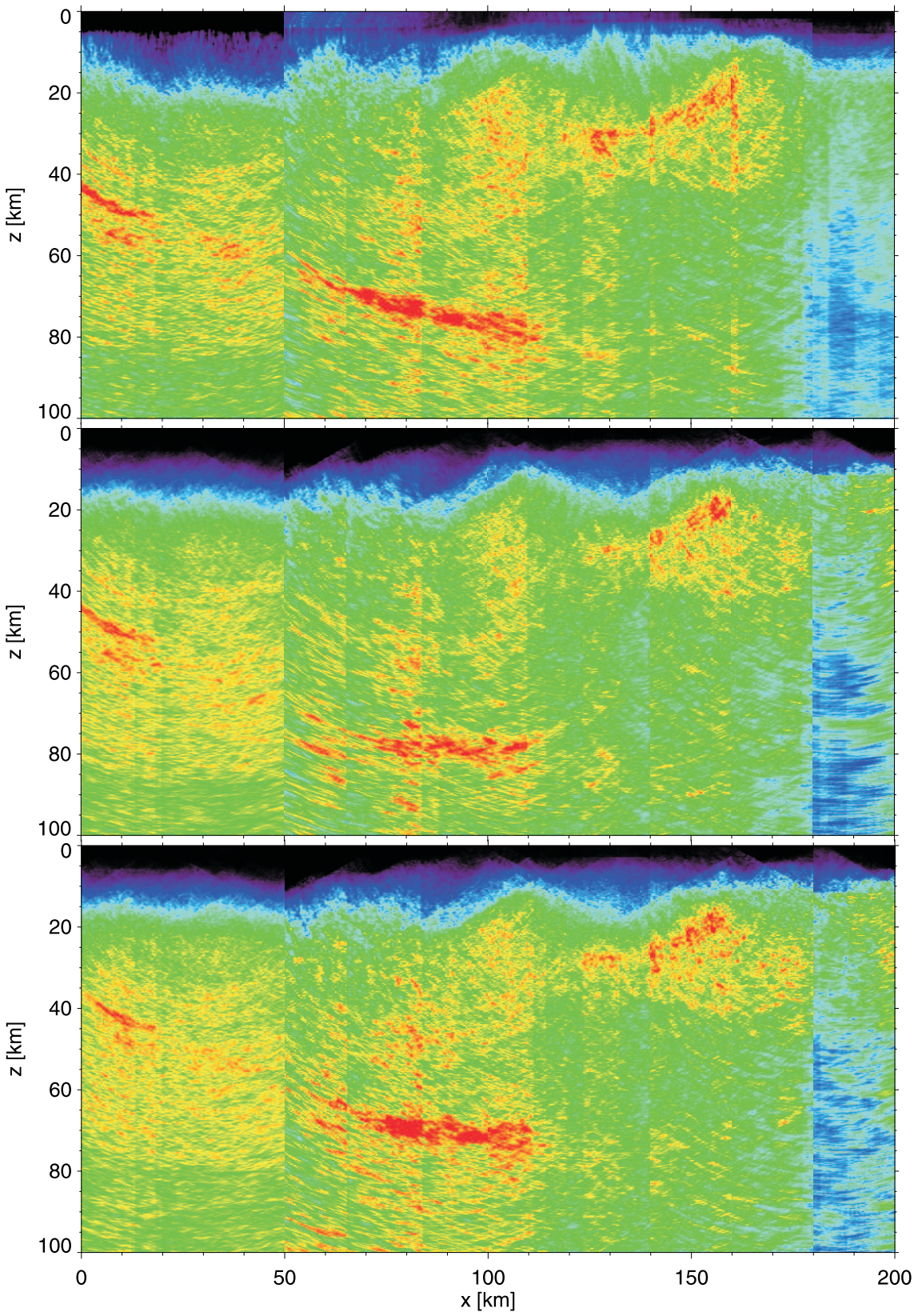

Figure 4.9: From top to bottom: The ANCORP sections calculated for model 1 (Lüth, 2000), for model 2 (Rietbrock and Haberland, 2001), and for model 3 (pers. comm. Koulakov, 2004).

boundary are located at depths of ca. 65 km and 75 km. The reflector disappears at around $x = 112$ km.

The comparison of the three depth images yields the following features. Section 1 (Fig. 4.9 top) provides the sharpest reflector image at the beginning of the profile. Both, the reflections from the top and bottom of the oceanic crust and from the continental Moho are sharp and pronounced compared to the images in the other sections. A comparison of the first 20 km in section 2 (Fig. 4.9, middle) and section 3 (Fig. 4.9, bottom) shows that section 2 provides a less diffuse and stronger image of the Nazca reflector than those visible in section 3. However, between $x = 20$ - 50 km neither section 2 nor section 3 reveals clear pronounced reflections. In the region between $x = 50$ - 110 km the Nazca reflector in section 1 shows a clear east dipping component, whereas in section 3 the same reflector shows a smaller dip angle. Both reflectors appear with similar reflection strength. In section 2, the Nazca reflector appears diffuse and almost horizontal, its shape becomes distorted. The depth of the Nazca reflector between $x = 70$ - 110 km differs in all three sections: In section 1, the upper and lower boundary are located at depths of 70 km and 80 km, in section 2 at $x = 75$ km and $x = 80$ km, respectively. The upper and the lower boundary of the same reflector in section 3 appear at depths of 65 km and 75 km, respectively.

The compilation of the recalculated images with the hypocenter locations are shown in Fig. 4.10. In image 1 the top of the oceanic crust is located at a depth of ca. 44 km at the beginning of the profile (top, Fig. 4.10, black dashed line). Its depth at $x = 85$ km is about 75 km. If this line is prolonged with the same dip down to greater depths, then the top of the oceanic crust at $x = 150$ km would be located at a depth of 97 km (pink dashed line). In this case, almost all hypocenters are located in the oceanic crust and mantle.

Section 2 indicates a different situation (middle, Fig. 4.10). Here, the top of the oceanic crust is again located at a depth of ca. 44 km at the beginning of the profile, but it reaches a depth of 80 km at $x = 80$ km. This is about 5 km deeper than in section 1. The prolongation would position the top of the oceanic crust at a depth of 110 km at $x = 150$ km (black dashed line). In this situation the hypocenters are located in the continental mantle and in the oceanic crust. If one assumes that the top of the hypocenters mark the top of the oceanic crust, then the corresponding position of the top of the oceanic crust has to be shifted upwards. Its hypothetic position is indicated by the pink dashed line. Thus, the dip angle of the oceanic crust has to decrease slightly between $x = 80$ - 150 km.

Section 3 yields another alternative (bottom, Fig. 4.10). Here, the top of the oceanic crust is located at a depth of ca. 37 km at the beginning of the profile and at a depth of 72 km

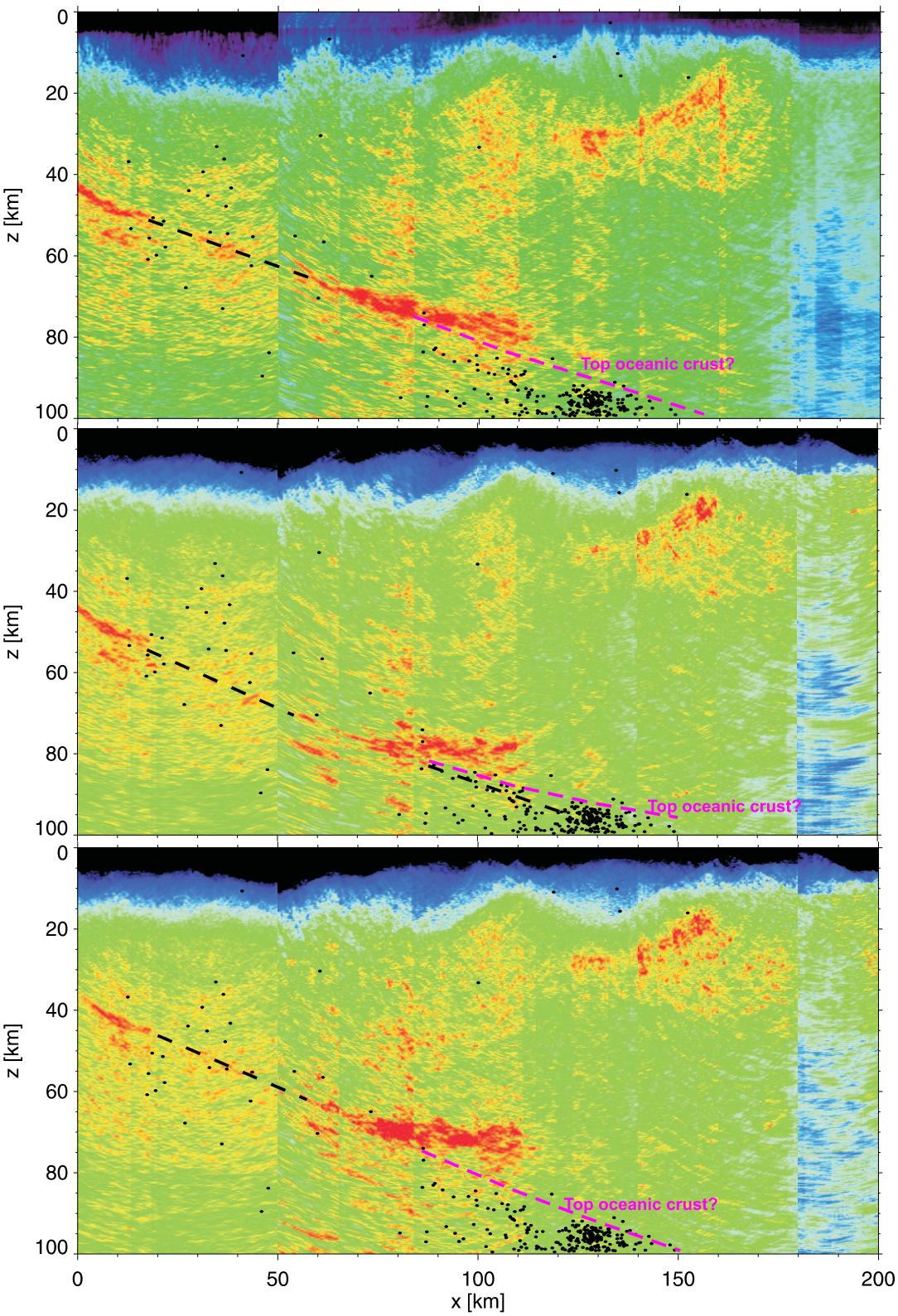

Figure 4.10: From top to bottom: The ANCORP sections calculated for model 1, for model 2 and for model 3 with hypocenter locations (black dots). The black dashed lines indicate the prolonged reflections from the top of the oceanic crust, the pink dashed lines the top of the oceanic crust interpreted from the hypocenter locations.

at $x = 80$ km. The prolongation of the top of the oceanic crust would then be located at a depth of ca. 100 km at $x = 150$ km. This in consequence means, that the hypocenters are located in the oceanic crust and mantle, similar to the situation observed in image 1. However, the observed dip of the oceanic crust is slightly steeper than in section 1 and section 2.

Resuming the results one can note that for model 1 the most pronounced and less disrupted reflections from the top and bottom of the oceanic crust in the beginning of the profile ($x = 0$ - 50 km) are obtained. Also, the reflections at $x = 0$ km are imaged at depths which are well constrained by reflections from wide-angle measurements (Patzwahl et al., 1999; Buske et al., 2002). Also, the observation that the hypocenters are located in the oceanic crust and mantle agrees with Rietbrock and Waldhauser (2004), who propose that all of the seismic activity is restricted to the oceanic plate. The depths of the reflections from the top and bottom of the oceanic crust obtained for model 2 are identical with the wide-angle reflections (Patzwahl et al., 1999), too. However, the Nazca reflector between $x = 70$ - 110 km appears distorted with a disrupted shape. The image of the Nazca reflector obtained for model 3 is similar to the reflector in section 1, except for the slightly differing dip angle, but the depths of the reflections from the top and bottom of the oceanic crust at $x = 0$ km are about 5 km less. Thus, it can be noted that model 2 appears accurate for imaging the first 50 km of the profile, but insufficient between $x = 70$ - 110 km. On the other hand the velocities in model 3 are too small at the beginning of the profile, but they provide an accurate image in the middle of the profile. Model 1 provides accurate images in both parts of the profile.

The differences in the velocity models 2 and model 3 are striking as both were derived from the tomographic inversion of the same earthquake data. It is assumed that the differences are due to the low data coverage and might be a result of the high dependence of the final model on the starting model. Recalculations using calibrated starting models, e.g. using a priori information from the refraction velocity model, seem meaningful to obtain a consistent tomography velocity model. Also, relocation of the hypocenters using model 3 might provide new insights into the deeper structures of the subduction zone.

4.2.4 RIS applied to ANCORP

In chapter 3 the application of RIS to synthetic data showed that imaging of reflection data in different frequency ranges recovers structural details that are not exposed in the seismic section using the whole frequency range. The numerical results showed that scat-